AIP | Applied Physics Letters

Probing Purcell enhancement in plasmonic nanoantennas by broadband luminescent Si quantum dots

Hiroshi Sugimoto, Shiho Yashima, Kenta Furuta, Asuka Inoue, and Minoru Fujii

Citation: Applied Physics Letters **108**, 241103 (2016); doi: 10.1063/1.4953829
View online: http://dx.doi.org/10.1063/1.4953829
View Table of Contents: http://scitation.aip.org/content/aip/journal/apl/108/24?ver=pdfcov
Published by the AIP Publishing

Probing Purcell enhancement in plasmonic nanoantennas by broadband luminescent Si quantum dots

Hiroshi Sugimoto, Shiho Yashima, Kenta Furuta, Asuka Inoue, and Minoru Fujii[a)]
Department of Electrical and Electronic Engineering, Graduate School of Engineering, Kobe University, Rokkodai, Nada, Kobe 657-8501, Japan

(Received 27 April 2016; accepted 1 June 2016; published online 14 June 2016)

Colloidal silicon quantum dots (Si QDs) with a very broad photoluminescence (PL) band are proposed as a probe to monitor the Purcell enhancement in a plasmonic nanostructure. Si QDs placed on an arbitrary plasmonic nanostructure enable us to determine the Purcell enhancement factors in a broad spectral range (600–900 nm). As a proof-of-concept experiment, a layer of Si QDs is spin-coated on gold film-over nanosphere structures, and the Purcell enhancement is quantitatively determined from the analyses of the PL spectra and the decay rates. The method proposed in this work provides a facile approach to quantitatively measure the performance of plasmonic substrates for PL and Raman enhancements. *Published by AIP Publishing.*
[http://dx.doi.org/10.1063/1.4953829]

Nanoscale plasmonic structures with a variety of shapes such as spheres, rods, disks and their arrays have been tailored for enhanced light-matter interactions.[1,2] The plasmonic nanostructures work as antennas, which enhance the excitation and emission rates of an emitter nearby. The latter is known as the Purcell effect,[3] which corresponds to the modification of the local density of photonic states (LDOS) at the position of an emitter. By carefully designing the plasmonic structure to maximize the excitation efficiency and the radiative decay rate, surface plasmon-enhanced photoluminescence (PL) has been demonstrated for various kinds of light emitting materials.[4–9] To optimize the PL enhancement, rigorous determination of the electromagnetic fields around the plasmonic structures and quantification of the Purcell factors are indispensable. This has been achieved by using electromagnetic calculations such as a finite element method, finite-difference time-domain, and boundary integral equations for well-defined plasmonic structures fabricated by electron-beam lithography.[2,10–12] On the other hand, most of the plasmonic structures ideal for large-scale and flexible applications do not have well-defined structures.[13,14] For example, metal island films,[13] which are often used as a facile plasmonic substrate, have large distributions in the size and shape of metal nanoparticles and gaps between them. The large distribution of the structural parameters makes modeling of the structure very difficult. Without accurate modeling of the structure, numerical calculations do not give correct electromagnetic field distributions. As a result, preparation parameters of large-scale plasmonic structures are usually determined in an empirical manner.

The purpose of this work is to develop a facile method to experimentally determine the Purcell enhancement factor of a plasmonic substrate in a wide wavelength range. An idea is to place nano-emitters onto a plasmonic substrate and study the emission dynamics. For this purpose, a plasmonic substrate has to be covered by a very thin layer of an emitter uniformly in a wide area by a low-temperature damage-free process. Furthermore, the emission band should be broad enough to cover the whole spectral range of the surface plasmon resonance of a plasmonic substrate, which is typically broader than 100 nm, and the emission should be efficient and stable in air. For the biological applications, the emission should be efficient and stable also in water-based solution, and the wavelength is preferably in the red to near-IR regions. An emitter having broad absorption bands is also favorable for the larger choice of the excitation wavelength.

In this paper, we propose all-inorganic colloidal silicon quantum dots (Si QDs) as an ideal material satisfying all these criteria.[15] Advantages of the all-inorganic Si QDs compared to commercially available II-VI or IV-VI QDs are the environmental friendliness and the higher stability of the luminescence in air and water. As a proof-of-concept experiment, we employ a metal-film over nanosphere (metal FON) structure plasmonic substrate, which has been widely used as the substrate for surface enhanced Raman scattering and PL.[16–18] FON substrates can be produced by a facile process and usually exhibit very high enhancement factors.[16–18] The structure is composed of interconnected metal half shells. Because of the large thickness gradience in the half shells and the variation of the shape and size of gaps between the half shells, accurate modeling of the structure is very difficult.[16–18] In this work, we cover the surface of gold (Au) FON substrates with a very thin layer of Si QDs by spin-coating and determine the Purcell factor in a wide wavelength range by the analyses of the PL dynamics. We demonstrate that the methodology presented in this work provides an alternative approach to determine the Purcell factor of a plasmonic substrate without numerical calculations.

In all-inorganic Si QDs used in this work, boron (B) and phosphorus (P) are very heavily doped, and a high B and P concentration shell is formed on the surface. The shell induces negative surface potential and prevents agglomeration of the QDs in polar solvents. Therefore, the codoped Si QDs are dispersible in alcohol without organic ligands. The detailed preparation procedure of the all-inorganic Si QDs is described in Refs. 15 and 19 and briefly summarized in the

[a)]Corresponding author e-mail: fujii@eedept.kobe-u.ac.jp

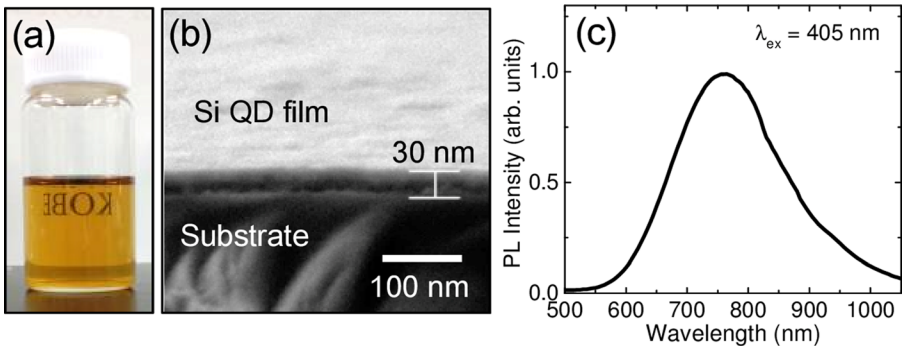

FIG. 1. (a) Photograph of colloidal dispersion of Si QDs (methanol solution). (b) SEM image of a spin-cast film of Si QDs on a Si substrate. (c) PL spectrum of the Si QD film excited at 405 nm.

supplementary material. In this work, we employ Si QDs with the average diameter of about 2.8 nm. Figure 1(a) shows a photograph of the colloidal dispersion of Si QDs, demonstrating the absence of scattering induced by agglomerates. Figure 1(b) shows a SEM image of a Si QD thin film on a Si wafer prepared by spin-coating the colloidal dispersion (2000 rpm, 15 μl of 0.9 mg/ml). A dense and smooth Si QD film is obtained. Figure 1(c) is the PL spectrum excited with monochromatized 405 nm light from a Xe lamp (Fluorolog-3, Horiba Jovin Yvon). The PL peak is at 750 nm with the full-width at half maximum (FWHM) of ~200 nm (440 meV).

Figure 2(a) shows a preparation procedure of a AuFON structure with a Si QD film. First, a 2D array of polystyrene (PS) spheres 350 nm in diameter is formed on a fused quartz substrate. The SEM image is shown in Figure 2(b). A 10 nm-thick titanium layer and a 200 nm-thick Au film are then deposited on the array by vacuum evaporation (Figure 2(c)). The Au film surface is treated by 3-methacryloxypropyltrimethoxysilane (3-MPTS). Finally, Si QD films with 30 and 60 nm in thicknesses are deposited by spin-coating (2000 rpm) the colloidal dispersion (1.4 mg/ml) one and two times, respectively. Hereafter, we denote Si QD films with the thicknesses of 30 and 60 nm as QD30 and QD60, respectively, and AuFON samples with these Si QD films as AuFON-QD30 and AuFON-QD60, respectively.

Figure 2(d) shows the absorptance (A) spectra defined by 1-R-T, where R and T are measured reflectance and transmittance, respectively, of the AuFON structures with and without Si QD films. The AuFON substrate exhibits a strong extinction at 620 nm arising from the surface plasmon resonance,[17,18,20,21] although the detailed origin of the resonance is still controversial due to the participation of both the localized and propagating surface plasmon resonances.[17,18,20,21] The spin-coating of the Si QD films results in a red-shift of the resonance peak due to the increase in the local refractive index (refractive index of Si QD film ~1.6); the degree of the shift depends on the thickness.

Figures 3(a) and 3(b) show the room temperature PL spectra of AuFON-QD30 and AuFON-QD60, respectively. PL spectra of 30 and 60 nm thick Si-QD films on flat Au substrates (AuF-QD30 and AuF-QD60, respectively) are also shown as references. The error bars in the spectra represent the standard deviations of the PL intensities obtained at 50 different points in each sample. In AuFON-QD30, the PL intensity is enhanced, and the peak exhibits a 20 nm blue-shift with respect to that of AuF-QD30. On the other hand, the PL peak shifts to the opposite direction in AuFON-QD60. The modification of the PL spectra is accompanied by significant shortening of the lifetimes. The representative decay curves detected at 750 nm using a gated intensified CCD (PI-Max, Princeton Instrument) are shown in the insets of Figs. 3(c) and 3(d). The excitation source is modulated 405 nm light. For the analysis of the decay curves, a stretched exponential function $I = I_0 \exp(-t/\tau)^{\beta}$ is used,[22] where τ is the decay constant and β is the stretching parameter. The average PL lifetime is defined as $\tau_{ave} = \tau\beta^{-1}\Gamma_E(\beta^{-1})$, where Γ_E is the Euler gamma function.[22] Figures 3(c) and 3(d) plot the PL decay rates ($1/\tau_{ave}$) of AuFON-QD30 and AuFON-QD60, respectively, as a function of detection wavelength. The decay rates are enhanced in the whole wavelength range in both samples.

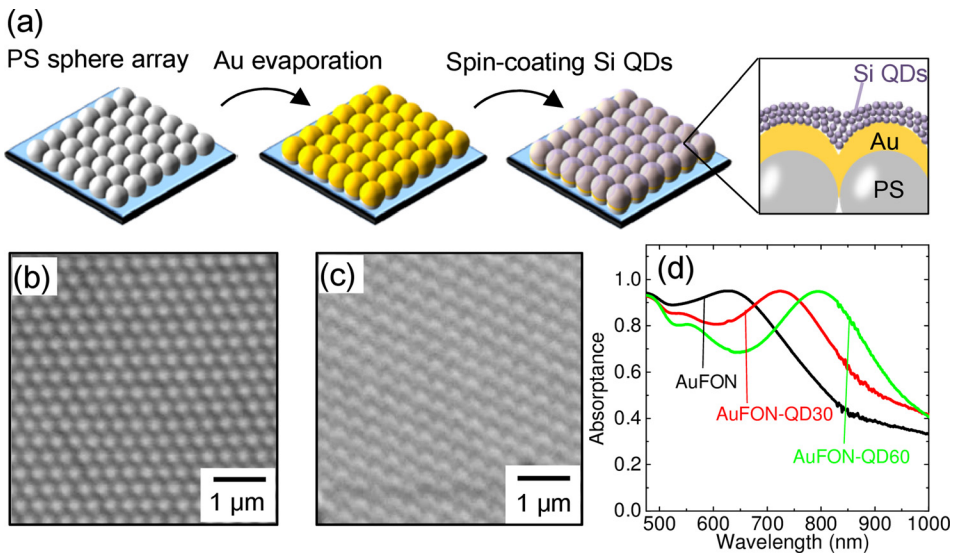

FIG. 2. (a) Fabrication procedure of a AuFON substrate with a Si QD film. SEM images of a 2D PS nanosphere array (b) before and (c) after Au deposition. (d) Absorptance spectra of AuFON structures with different thickness Si QD films.

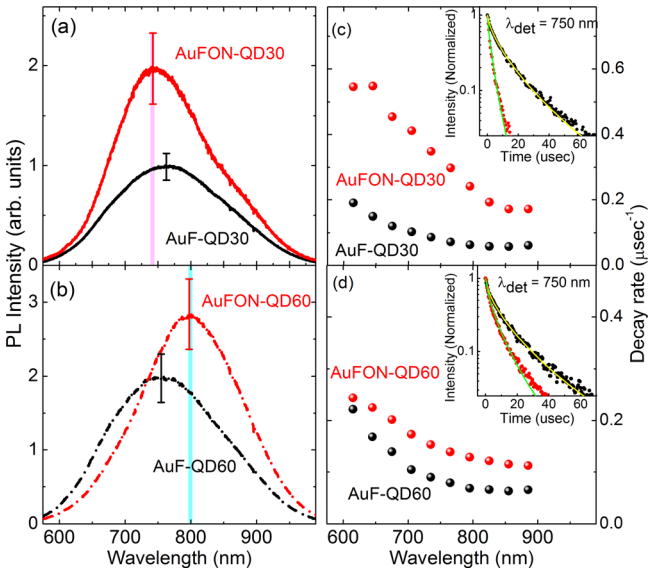

FIG. 3. (a) and (b) PL spectra and (c) and (d) decay rates of AuF-QD30 and 60 (black) and AuFON-QD30 and 60 (red). Insets of (c) and (d) show representative PL decay curves of AuF-QD30 and 60 (black) and AuFON-QD30 and 60 (red) detected at 750 nm with the fitting curves.

It should be noted here that the decay rates of Si QDs on a flat Au film are also modified from those of colloidal Si QDs. The enhancement factors of the radiative and nonradiative decay rates of dipoles placed on a flat Au film with respect to those in vacuum can be analytically calculated by the method developed by Chance *et al.*[23,24] The calculated normalized decay rates for AuF-QD30 and AuF-QD60 are shown in the supplementary material (Figure S1).[25] In the calculation, emitters are treated as isotropic dipoles uniformly positioned within the regions of 30 and 60 nm from the Au surface for AuF-QD30 and AuF-QD60, respectively. The normalized radiative rate is below unity in the whole wavelength range due to the interference between the incident and reflected fields, while the nonradiative decay rate is very large, especially in the short wavelength region. This is due to the coupling of an emitter with the surface plasmon polariton and the lossy surface wave modes in the metal. We will take into account these results for the determination of the Purcell enhancement in the AuFON structure.

Figure 4(a) shows the ratio of the decay rates between AuFON (Γ_{FON}) and AuF (Γ_F) for QD30 (black) and QD60 (red) as a function of the emission wavelength. The red dashed lines are the extinction spectra of the corresponding AuFON structures. The enhancement factors (Γ_{FON}/Γ_F) have a peak at the wavelength of the extinction peak. The maximum enhancement factors reach approximately 4.2 at 760 nm for QD30 and 1.9 at 800 nm for QD60. Figure 4(b) shows the ratio of the PL intensity ($\frac{I_{FON}}{I_F}$) between AuFON (I_{FON}) and AuF (I_F) for QD30 (black) and QD60 (red). A peak can be seen near the extinction peak.

The measured PL intensity ratio ($\frac{I_{FON}}{I_F}$) is expressed as the product of the ratios of the excitation cross-section ($\frac{\sigma_{FON}}{\sigma_F}$), the quantum efficiency ($\frac{Q_{FON}}{Q_F}$), and the light collection efficiency ($\frac{\eta_{FON}}{\eta_F}$); $\frac{I_{FON}}{I_F} = \frac{Q_{FON}}{Q_F}\frac{\sigma_{FON}}{\sigma_F}\frac{\eta_{FON}}{\eta_F}$.[14,26] Among them, $\frac{\sigma_{FON}}{\sigma_F}$ can be approximated to be 1, because the excitation wavelength (405 nm) is far from the surface plasmon resonance wavelengths of the AuFON. The collection efficiency also does not change largely between AuFON and AuF. Therefore, the measured PL enhancement originates mainly from the quantum efficiency enhancement.

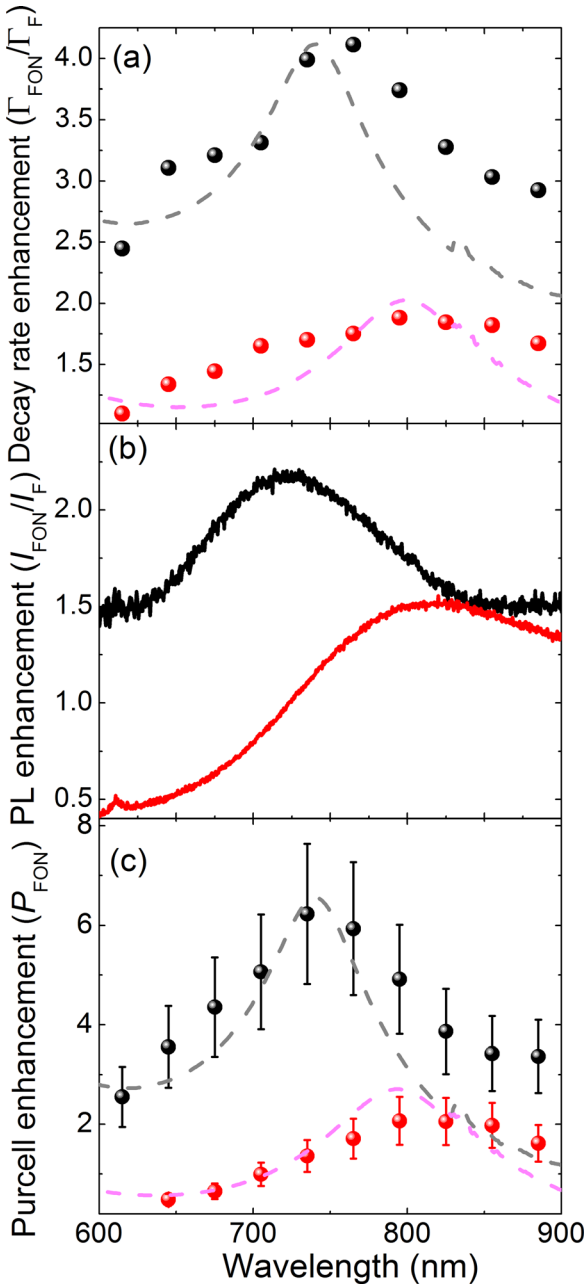

FIG. 4. (a) Decay rate (Γ_{FON}/Γ_F) and (b) PL (I_{FON}/I_F) enhancements of AuFON-QD30 (black) and AuFON-QD60 (red) with respect to those of AuF-QD30 and AuF-QD60, respectively, as a function of emission wavelength. (c) Purcell enhancement spectra (P_{FON}) of AuFON-QD30 (black) and AuFON-QD60 (red).

In the AuFON and AuF structures, the radiative decay rates are modified to $P_{FON}\,\gamma_r$ and $P_F\,\gamma_r$, where P_{FON} and P_F are the Purcell factors, respectively, and γ_r is the intrinsic radiative rate of Si QDs in vacuum. By using the measured PL decay rates (Γ_{FON} and Γ_F), Q_{FON} and Q_F can be expressed as $P_{FON}\,\gamma_r/\Gamma_{FON}$ and $P_F\,\gamma_r/\Gamma_F$, respectively. The PL intensity ratio is thus

$$\frac{I_{FON}}{I_F} = \frac{Q_{FON}}{Q_F} = \frac{P_{FON}}{P_F}\frac{\Gamma_F}{\Gamma_{FON}}. \quad (1)$$

Since I_{FON}/I_F and Γ_F/Γ_{FON} are experimentally determined and P_F can be calculated by an analytical method, P_{FON} is obtained from Eq. (1). Figure 4(c) shows P_{FON} obtained for AuFON-QD30 and QD60. In AuFON-QD30, P_{FON} has a peak around 750 nm, while in AuFON-QD60, it has a peak around 800 nm. In both cases, the shape of the P_{FON} spectra coincides with the extinction spectra very well. This proves the validity of our analysis to determine the Purcell factor of metal nanostructures. The Purcell enhancement of AuFON-QD30 exceeds 6 at the maximum, while it is around 2 in AuFON-QD60. The different values of the maximum P_{FON} between the two samples can be explained by strong dependence of the Purcell factor of plasmonic nanostructures on the distance from the surface.[27]

In conclusion, we have proposed a method to quantitatively determine the Purcell enhancement factor of metal nanostructures utilizing the broadband luminescence from colloidal Si QDs. As a test structure, we employed AuFON structures and determined the Purcell enhancement factors quantitatively in a wide wavelength range from the analyses of the PL spectra and the decay dynamics of Si QDs placed on the AuFON structures. Since a thin layer of Si QDs can be placed on an arbitrary shape metal nanostructure by spin-coating, screen printing, etc., the present method is very versatile and can be applied to plasmonic nanostructures that are hard to be modeled accurately for numerical calculations.

This work was partly supported by 2014 JSPS Bilateral Joint Research Projects (Japan-Czech Republic), 2015 JST Visegrad Group (V4)-Japan Joint Research Project on Advanced Materials and KAKENHI (16H03828). H.S. acknowledges the support from the Grant-in-Aid for JSPS Fellows (No. 26-3120).

[1]V. Giannini, A. I. Fernández-Domínguez, S. C. Heck, and S. A. Maier, Chem. Rev. **111**, 3888 (2011).
[2]G. M. Akselrod, C. Argyropoulos, T. B. Hoang, C. Ciracì, C. Fang, J. Huang, D. R. Smith, and M. H. Mikkelsen, Nat. Photonics **8**, 835 (2014).
[3]E. M. Purcell, Phys. Rev. **69**, 674 (1946).
[4]K. Tanaka, E. Plum, J. Y. Ou, T. Uchino, and N. I. Zheludev, Phys. Rev. Lett. **105**, 227403 (2010).
[5]E. Cohen-Hoshen, G. W. Bryant, I. Pinkas, J. Sperling, and I. Bar-Joseph, Nano Lett. **12**, 4260 (2012).
[6]J. S. Biteen, N. S. Lewis, H. A. Atwater, H. Mertens, and A. Polman, Appl. Phys. Lett. **88**, 131109 (2006).
[7]P. P. Pompa, L. Martiradonna, A. Della Torre, F. Della Sala, L. Manna, M. De Vittorio, F. Calabi, R. Cingolani, and R. Rinaldi, Nat. Nanotechnol. **1**, 126 (2006).
[8]D. Nepal, L. F. Drummy, S. Biswas, K. Park, and R. A. Vaia, ACS Nano **7**, 9064 (2013).
[9]H. Sugimoto, T. Chen, R. Wang, M. Fujii, B. M. Reinhard, and L. Dal Negro, ACS Photonics **2**, 1298 (2015).
[10]T. B. Hoang, G. M. Akselrod, C. Argyropoulos, J. Huang, D. R. Smith, and M. H. Mikkelsen, Nat. Commun. **6**, 7788 (2015).
[11]J. M. McMahon, A.-I. Henry, K. L. Wustholz, M. J. Natan, R. G. Freeman, R. P. Van Duyne, and G. C. Schatz, Anal. Bioanal. Chem. **394**, 1819 (2009).
[12]U. Hohenester and J. Krenn, Phys. Rev. B **72**, 195429 (2005).
[13]T. Aisaka, M. Fujii, and S. Hayashi, Appl. Phys. Lett. **92**, 132105 (2008).
[14]J. S. Biteen, D. Pacifici, N. S. Lewis, and H. A. Atwater, Nano Lett. **5**, 1768 (2005).
[15]H. Sugimoto, M. Fujii, K. Imakita, S. Hayashi, and K. Akamatsu, J. Phys. Chem. C **116**, 17969 (2012).
[16]W. C. Lin, L. S. Liao, Y. H. Chen, H. C. Chang, D. P. Tsai, and H. P. Chiang, Plasmonics **6**, 201 (2011).
[17]C. Farcău and S. Aştilean, Appl. Phys. Lett. **95**, 193110 (2009).
[18]J. Lee, Q. Zhang, S. Park, A. Choe, Z. Fan, and H. Ko, ACS Appl. Mater. Interfaces **8**, 634 (2016).
[19]H. Sugimoto, M. Fujii, K. Imakita, S. Hayashi, and K. Akamatsu, J. Phys. Chem. C **117**, 11850 (2013).
[20]C. Farcau and S. Astilean, J. Phys. Chem. C **114**, 11717 (2010).
[21]P. Krohne-Nielsen, S. Novikov, J. Beermann, P. Morgen, S. Bozhevolnyi, and O. Albrektsen, Opt. Express **20**, 534 (2012).
[22]C. P. Lindsey and G. D. Patterson, J. Chem. Phys. **73**, 3348 (1980).
[23]R. Chance, A. Prock, and R. Silbey, Adv. Chem. Phys. **1**, 65 (2007).
[24]W. L. Barnes, J. Mod. Opt. **45**, 661 (1998).
[25]See supplementary material at http://dx.doi.org/10.1063/1.4953829 for Figure S1.
[26]M. Y. Shalaginov, S. Ishii, J. Liu, J. Liu, J. Irudayaraj, A. Lagutchev, A. V. Kildishev, and V. M. Shalaev, Appl. Phys. Lett. **102**, 173114 (2013).
[27]S. Jin, E. Demarco, M. J. Pellin, O. K. Farha, G. P. Wiederrecht, and J. T. Hupp, J. Phys. Chem. Lett. **4**, 3527 (2013).